*Proceedings of The Thirteenth (2003) International Offshore and Polar Engineering Conference*
*Honolulu, Hawaii, USA, May 25−30, 2003*

*ISBN 1−880653-60−5 (Set); ISSN 1098−6189 (Set)*

# Numerical Simulations of Three-dimensional Wave Breaking by Coupling of a VOF Method and a Boundary Element Method

*B. Biausser, S.T. Grilli, P. Fraunié*

LSEET, Université de Toulon et du Var / Principia R.D, La Garde / La Ciotat, France

Dpt. of ocean Engineering, University of Rhode Island, Narragansset RI, USA

LSEET, Université de Toulon et du Var, La Garde , France

## ABSTRACT

In this paper, we describe the development and validation of a numerical model based on coupling a higher-order Boundary Element Method (BEM) solution of fully nonlinear potential flow equations to a Volume Of Fluid (VOF) solution of Euler equations, in three-dimensions (3-D). In the model, the BEM solution is used to initialize the VOF/Euler computations. Numerical simulations of breaking waves on sloping beaches for 2-D (using an earlier model) and 3-D flows are carried out.

Keywords: Breaking ocean waves; nonlinear surface waves; Segment Lagrangian Volume of Fluid Method; Boundary Element Method; Numerical Wave Tank.

## INTRODUCTION

The study of breaking waves is of prime importance in many ocean and naval engineering applications. Despite significant progress in recent years, the understanding of wave breaking is still quite incomplete. Due to the development of modern computers, direct Computational Fluid Dynamics (CFD) simulations of wave breaking can now be carried out and used to gain insight into this complex process. In such problems, one numerically solves full fluid dynamics equations, together with nonlinear dynamic and kinematic free surface boundary conditions, and other boundary conditions to represent solid surfaces or open boundaries. Models based on potential flow equations (BEM) are very accurate and efficient for simulating wave shoaling over arbitrary bottom topography, up to overturning (Grilli et al., 1994, 1996, 1997, and 2001). Such models, however, are unable to deal with interface reconnections and large deformations occurring during wave breaking. To overcome this difficulty, Guignard et al. (1999) proposed to use a BEM solution as an initial solution for a VOF/Navier-Stokes (or Euler) model, in which wave breaking could be fully simulated. These coupled BEM/VOF computations were performed in 2D. Here, the same approach is applied to 3D problems, through coupling of Grilli et al.'s (2001) 3D-BEM model to the interface tracking, SL-VOF 3D method of Biausser et al. (2002). In the first section, the mathematical formulation is briefly presented. The second section deals with the numerical methods., with details of the interface tracking SL-VOF method, and coupling with the BEM formulation for wave breaking. Finally, two simple applications of quasi-2-D wave breaking simulations with the 3D-BEM/SL-VOF model are presented. More simulations for truly 3-D breaking waves are presented and their internal kinematics analyzed in detail in a companion paper (Biausser et al., 2003).

## MATHEMATICAL FORMULATION

### BEM formulation

Equations for fully nonlinear potential flows with a free surface are listed below. The velocity potential $\phi(\mathbf{x},t)$ is introduced to describe inviscid irrotational 3D flows, in Cartesian coordinates $\mathbf{X}=(x,y,z)$, with z the vertical upward direction ($z = 0$ at the undisturbed free surface), and the fluid velocity is expressed as $\mathbf{u} = \nabla\phi$. Continuity equation in the fluid domain $\Omega(t)$ with boundary $\Gamma(t)$ is Laplace's equation

$$\nabla^2 \phi = 0. \tag{1}$$

The corresponding three-dimensional free-space Green's function is defined as

$$G(\mathbf{x},\mathbf{x}_l) = \frac{1}{4\pi r} \qquad \text{with} \qquad \frac{\partial G}{\partial n}(\mathbf{x},\mathbf{x}_l) = -\frac{1}{4\pi}\frac{\mathbf{r}.\mathbf{n}}{r^3}, \tag{2}$$

with, $r = |\mathbf{X} - \mathbf{X}_l|$ the distance from the source point $\mathbf{X}$ to the field point $\mathbf{X}_l$ (both on boundary $\Gamma$), and $\mathbf{n}$ the outward unit vector normal to the boundary at point $\mathbf{X}$.

Green's second identity transforms Eq. (1) into the Boundary Integral Equation (BIE)

$$\alpha(\mathbf{x}_l)\phi(\mathbf{x}_l) = \int_\Gamma \left[ \frac{\partial \phi}{\partial n}(\mathbf{x}) G(\mathbf{x},\mathbf{x}_l) - \phi(\mathbf{x}) \frac{\partial G}{\partial n}(\mathbf{x},\mathbf{x}_l) \right] d\Gamma, \tag{3}$$

where $\alpha(\mathbf{x}_l) = \frac{1}{4\pi}\theta_l$ and $\theta_l$ is the exterior solid angle at point $\mathbf{X}_l$.

The boundary is divided into various parts in which different boundary conditions are specified. On the free surface $\Gamma_f(t)$, $\phi$ satisfies the nonlinear kinematic and dynamic boundary conditions,

$$\frac{D\mathbf{R}}{Dt} = \mathbf{u} = \nabla\phi \quad , \tag{4}$$

$$\frac{D\phi}{Dt} = -gz + \frac{1}{2}\nabla\phi.\nabla\phi - \frac{p}{\rho} \ , \tag{5}$$

respectively, in a Mixed Eulerian-Lagrangian formulation (MEL), with **R** the position vector of a fluid particle on the free surface, $g$ the acceleration due to gravity, $p$ the atmospheric pressure, $\rho$ the fluid density and $D/Dt = \partial/\partial t + \nabla\phi.\nabla$ the Lagrangian time derivative. The effects of surface tension are neglected.

For simple waves, such as solitary waves, the free surface shape, potential and normal velocity of the incident wave are specified at time $t = 0$ on the free surface based on Tanaka's method (Tanaka,1986). More complex incident wave conditions can be specified using numerical wavemakers (e.g., Grilli and Horrillo, 1997, 1999; Brandini and Grilli, 2001).

On the bottom boundary, $\Gamma_b$ and on other fixed parts of the boundary, a no-flow condition is prescribed as

$$\frac{\partial\phi}{\partial n} = 0. \tag{6}$$

Once the BIE (3) is solved, the solution within the domain can be explicitly calculated, based on boundary values. Using Eq. (3), for instance, the internal velocity at the interior point $\mathbf{X}_i$ is given by Eqs. (7) and (8), respectively, below

$$\mathbf{u}\,(\mathbf{x}_i) = \nabla\phi(\mathbf{x}_i) = \int_\Gamma \left[\frac{\partial\phi}{\partial n}(\mathbf{x})Q(\mathbf{x},\mathbf{x}_i) - \phi(\mathbf{x})\frac{\partial Q}{\partial n}(\mathbf{x},\mathbf{x}_i)\right] d\Gamma \ , \tag{7}$$

$$Q(\mathbf{x},\mathbf{x}_i) = \frac{1}{4\pi r^3}\mathbf{r} \ , \ \frac{\partial Q}{\partial n}(\mathbf{x},\mathbf{x}_i) = \frac{1}{4\pi r^3}\left[\mathbf{n} - 3(\mathbf{r}.\mathbf{n})\frac{\mathbf{r}}{r}\right] , \tag{8}$$

where $r$ denotes the distance from the boundary point **X** to $\mathbf{X}_i$.

### Navier-Stokes Formulation

The 3D Navier-Stokes equations for two-phase (air-water) flows are given as follows, in a semi-conservative curvilinear formulation:

$$\frac{1}{J}\frac{\partial W}{\partial t} + \frac{\partial F}{\partial \xi} + \frac{\partial G}{\partial \eta} + \frac{\partial H}{\partial \chi} = \frac{R}{J} + \frac{T}{J} \tag{9}$$

where $F,G$ and $H$ are flux terms, $R$ is the volumetric force source term and $T$ the surface tension source term, with :

$$F = \frac{1}{J}\begin{pmatrix} \rho\tilde{u} \\ \rho\tilde{u}u + \xi_x p - \vec{\nabla}(\xi).\vec{\tau}_x \\ \rho\tilde{u}v + \xi_y p - \vec{\nabla}(\xi).\vec{\tau}_y \\ \rho\tilde{u}w + \xi_z p - \vec{\nabla}(\xi).\vec{\tau}_z \end{pmatrix}; G = \frac{1}{J}\begin{pmatrix} \rho\tilde{v} \\ \rho\tilde{v}u + \eta_x p - \vec{\nabla}(\eta).\vec{\tau}_x \\ \rho\tilde{v}v + \eta_y p - \vec{\nabla}(\eta).\vec{\tau}_y \\ \rho\tilde{v}w + \eta_z p - \vec{\nabla}(\eta).\vec{\tau}_z \end{pmatrix};$$

$$H = \frac{1}{J}\begin{pmatrix} \rho\tilde{w} \\ \rho\tilde{w}u + \chi_x p - \vec{\nabla}(\chi).\vec{\tau}_x \\ \rho\tilde{w}v + \chi_y p - \vec{\nabla}(\xi).\vec{\tau}_y \\ \rho\tilde{w}w + \chi_z p - \vec{\nabla}(\xi).\vec{\tau}_z \end{pmatrix}; W = \begin{pmatrix} 0 \\ \rho u \\ \rho v \\ \rho w \end{pmatrix}; T = \begin{pmatrix} 0 \\ \sigma K n_x \\ \sigma K n_y \\ \sigma K n_z \end{pmatrix}; R = \begin{pmatrix} 0 \\ \rho f_x \\ \rho f_y \\ \rho f_z \end{pmatrix}$$

$$\tilde{u} = \xi_x u + \xi_y v + \xi_z w \, ; \, \tilde{v} = \eta_x u + \eta_y v + \eta_z w \, ; \, \tilde{w} = \chi_x u + \chi_y v + \chi_z w \, ;$$

$$J = \frac{\partial(\xi,\eta,\chi)}{\partial(x,y,z)}$$

$$\vec{\tau}_x = \overline{\overline{\tau}}.\vec{e}_x \quad \vec{\tau}_y = \overline{\overline{\tau}}.\vec{e}_y \quad \vec{\tau}_z = \overline{\overline{\tau}}.\vec{e}_z \quad \overline{\overline{\tau}} = \mu(\vec{\nabla}\vec{U} + \vec{\nabla}^t\vec{U}) \tag{10}$$

where $(\xi,\eta,\chi)$ denote curvilinear coordinates, $J$ is the Jacobian matrix of the coordinate transformation, $\sigma$ is the surface tension coefficient, $K$ the surface curvature and $\vec{n} = (n_x, n_y, n_z)$ the normal vector to the interface. Additionally, $(u,v,w)$ are the Cartesian velocity components for each phase, $(\tilde{u},\tilde{v},\tilde{w})$ the contravariant velocity components, $p$ the pressure, $\rho$ the density, $\mu$ the molecular viscosity, and $\overline{\overline{\tau}}$ the viscous stress tensor. Nevertheless, the viscocity is neglected in this study so that Euler equations are solved.

## NUMERICAL MODELS

### Numerical method for the BEM model

***Time integration***

A second-order explicit time stepping scheme, based on Taylor series expansions, is used to update both the position **R** and the velocity potential $\phi$ on the free surface, as

$$\mathbf{R}(t+\Delta t) = \mathbf{R} + \Delta t\frac{D\mathbf{R}}{Dt} + \frac{\Delta t^2}{2}\frac{D\mathbf{R}}{Dt} + O(\Delta t^3), \tag{11}$$

$$\phi(t+\Delta t) = \phi + \Delta t\frac{D\phi}{Dt} + \frac{\Delta t^2}{2}\frac{D\phi}{Dt} + O(\Delta t^3) \ , \tag{12}$$

where $\Delta t$ is the varying time step and all terms in the right-hand sides are evaluated at time $t$ (see Grilli et al., 2001, for detailed expressions). The time step $\Delta t$ in Eqs. (11) and (12) is adaptively selected at each time as

$$\Delta t = C_0\frac{\Delta r^{\min}}{\sqrt{gh}} \quad , \tag{13}$$

where $C_0$ denotes the mesh Courant number, $\Delta r^{\min}$ is the instantaneous minimum distance between two neighboring nodes on $\Gamma_f$ and $h$ is a characteristic depth.

Global accuracy of the numerical scheme can be assessed at any time by checking the conservation of volume and energy in the computational domain.

***Boundary discretization***

A high-order Boundary Element Method (BEM) is used to discretize and solve numerically the BIEs for $\phi$ and $\partial\phi/\partial t$ (Grilli et al., 2001). The boundary is represented by a series of collocation nodes, in between which, two-dimensional elements are defined to express the local interpolation of the solution. Thus, within each element, the boundary geometry and field variables are interpolated using polynomial shape functions. A robust treatment requires defining elements, which are both high-order within their area of definition and at least locally $C_2$ continuous at their edges. For this purpose, an extension of the so-called cubic middle-interval-interpolation (MII) method introduced by Grilli and Subramanya (1996) has been developed in the 3D model. The boundary elements are 4x4-node quadrilaterals associated with bi-cubic shape functions. The discretized boundary integrals are evaluated for each collocation node by numerical integration.

A special treatment of singular terms is applied for weakly singular integrals in the BIE (3). As the linear algebraic system resulting from the discretization of Eq. (3) is in general fully populated and non-symmetric, a generalised minimal residual (GMRES) algorithm with preconditioning is used for the numerical solution at each time step (Xü and Yue, 1992). Accuracy is increased in regions of high variability by redistributing nodes on the free surface, using a regridding technique based on the BEM shape functions.

## Numerical method for the VOF/Navier-Stokes model

***Pseudo-compressibility method***

Time discretization in the Navier-Stokes model is based on a fully implicit second-order finite difference scheme. The solution of the non-linear system at time step $n$+1 is based on the "pseudo-compressibility method" (Viviand 1980, De Jouëtte et al. 1991). In this method, a time-like variable $\tau$, called pseudo-time, is introduced in Eq. (9). This adds pseudo-unsteady terms, which are derivatives of the unknowns at time level $n$+1, with respect to $\tau$. Considering semi-discretized equations only, at time level $n$+1, the system is then written:

$$\frac{1}{J}\frac{\partial \tilde{W}^{n+1}}{\partial \tau}+\frac{1}{J}\frac{3W^{n+1}-4W^{n}+W^{n-1}}{2\Delta t}+\left(\frac{\partial F}{\partial \xi}\right)^{n+1}+\left(\frac{\partial G}{\partial \eta}\right)^{n+1}+\left(\frac{\partial H}{\partial \chi}\right)^{n+1}= \frac{R}{J}^{n+1}+\frac{T}{J}^{n+1} \tag{14}$$

with

$$\tilde{W}=\begin{pmatrix}\tilde{\rho}\\ \tilde{\rho}u\\ \rho v\\ \tilde{\rho}w\end{pmatrix}$$

The pseudo-unsteady terms in $\tilde{W}$ involve a new unknown, $\tilde{\rho}$, called pseudo-density, which is constrained to remain positive. The pressure is calculated as a function of $\tilde{\rho}$ through an additional pseudo-state equation:

$$p^{n+1}=\rho(U_0^2+\lambda U_n^2)\ln\left(\frac{\tilde{\rho}}{\rho}\right)^{n+1} \tag{15}$$

The choice of an optimal pseudo-state equation is discussed in Viviand (1995).

The system of Eqs. (14),(15) is integrated step-by-step in pseudo-time variable, with an explicit five step Runge-Kutta scheme, associated with an implicit residual smoothing technique, up to convergence towards the numerical solution at time level $n$+1. This system is hyperbolic with respect to $\tau$ and is formally very close to Navier-Stokes equations for compressible flows, due to the presence of similar terms in $\tilde{\rho}$, in both continuity and momentum equations. The spatial discretization is based on an adaptation of the finite volume method for multiple-block curvilinear deforming grids, using a centred scheme with artificial viscosity (Jameson et al. 1981). This procedure allows avoiding uncoupling between odd and even cells. The maximum value of the pseudo-time step is fixed by a local cell CFL stability criterion (local time step technique). The method is unconditionally stable with respect to the physical time step. Finally this method is especially robust to deal with two-phase flows exhibiting a high liquid-gas density ratio.

***Interface tracking VOF method***

The VOF method (Hirt and Nichols, 1981) uses the volumetric fraction $C$ of the denser fluid in grid cells, to track interface locations. This method is convenient for high deformations of interfaces. Unlike the BEM method, the VOF method can deal with topological reconnections or de-connections. More specifically, we use the Segment Lagrangian Volume Of Fluid method (SL-VOF; Guignard et al. 1999, Biausser et al. 2001,2002), for 2-D and 3-D flows, which is based on a piecewise linear modeling of the interface (PLIC) and a Lagrangian advection scheme. At the beginning of a time step, say $n$, the VOF field $C$ is used to define a piecewise linear interface representation (segments in 2-D or portions of planes in 3-D). To do so, in each computational cell, the normal vector **n** to the interface plane, defined as $-\nabla C^n$, is first evaluated using finite differences. Once this direction is known, the segment is translated in the cell in order to satisfy the VOF cell value. Lagrangian markers $M_i$ are specified on each segment/plane and, in each cell, these are advected based on the flow velocity computed in the Navier-Stokes solver. The segment corner velocities are calculated from the velocity at the center of each cell using bilinear interpolation. The advection is carried out with a first order Lagrangian scheme

$$\mathbf{x}(t+\Delta t)=\mathbf{x}(t)+\Delta t.\mathbf{u}\ , \tag{16}$$

where **x** denotes the corner position, **u** the corner velocity and $\Delta t$ the time step.

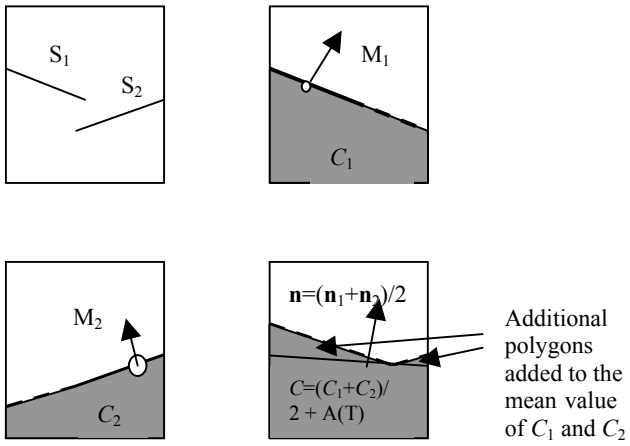


Figure 1: computation of $C^{n+1}$ for an A type cell with 2 segments (no reconnection). $S_1$ defines $C_1$, $S_2$ defines $C_2$, $C$ is the mean value of $C_1$ and $C_2$, plus the areas of the additional triangles

To each marker $M_i$, we associate the normal vector $\mathbf{n}_i$ of the segment to which the marker belongs. After advection, we find two possible types of cells:

- A type cells containing at least one marker
- B type cells without any marker

Let us consider an A type cell (Fig. 1). To the marker $M_i$ corresponds a value $C_i$ calculated according to the PLIC method. As there are several portions of segments (for 2-D cases) in the cell, it is necessary to determine whether the cell is growing full (interface reconnection) or not. To do so, a test is made on the value of, $pr_{ij} = \mathbf{n}_i.\mathbf{n}_j$, where i and j describe the markers present in the cell. If all the $pr_{ij}$'s are positive, then the new value of the VOF field $C$ will be the mean of the $C_i$'s in the cell, to which is added or subtracted the areas of additional polygons A(T).

If at least one $pr_{ij}$ is negative, a reconnection of interfaces could occur in the cell. Thus, segments could overlap each other so that the cell would become full of liquid phase. This is the case when the sum of the $C_i$'s is greater than 1, and $C^{n+1}$ is then specified to be 1 (Fig. 2). If the sum of the $C_i$'s is less than 1, $C^{n+1}$ is computed in the same way as above.

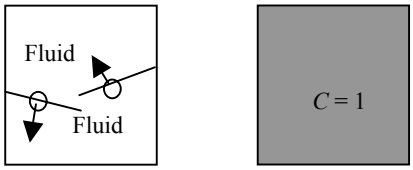


Figure 2: computation of $C^{n+1}$ for a A type cell with 2 segments (reconnection)

Let us now consider a B type cell (Fig. 3). There are again two possibilities: (i) either the cell did not contain any segment before advection of the interface, and thus the value of $C$ is not modified; (ii) or the cell has lost its interface during the current time step. In case (ii), one has to detect whether the cell becomes empty or full of the denser fluid, after advection. A test is made on the value of, $pr = \mathbf{n.d}$ where $\mathbf{d}$ is the displacement of the center of the segment during advection. The cell is deemed full if $pr > 0$ and empty if not (Fig. 3).

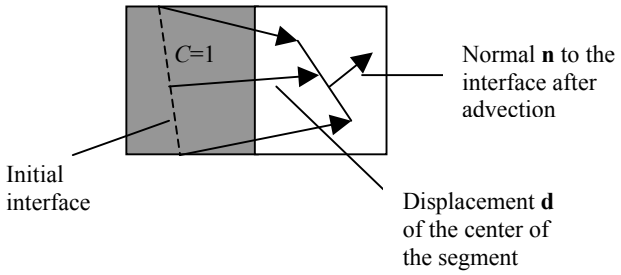


Figure 3: computation of $C^{n+1}$ for a B type cell case with, $\mathbf{n}.\mathbf{d} > 0$

For 3-D problems, the principle of the method is the same but the geometrical relationships are more complex and based on the displacement of planes rather than segments (see Biausser et al., 2002). The piecewise linear modelling of the interface again makes it possible to track interfaces with complex and/or distorted shape with good accuracy.

The Lagrangian advection performed in cells in 2-D or 3-D allows to use large CFL values, which reduces computational time.

***Coupling with BEM formulation***

The VOF/Navier Stokes model can simulate breaking and post-breaking waves on slopes. This model, however, is very computationally demanding and requires to be applied on sufficiently fine grids, as compared to the scale of variation of physical phenomena to be simulated. Moreover, the VOF method may induce unwanted numerical dissipation, when applied to waves over long distances of propagation, which leads to non-physical loss of wave energy. As discussed in the introduction, the coupling of the VOF and BEM models provides a more efficient and accurate means of simulating breaking waves over slopes.The BEM is accurate and efficient for modeling wave shoaling and can thus be used to propagate waves over the slope, up to very close to breaking. The BEM solution is then used to initialize the VOF/Navier-Stokes solver on a refinied grid, limited to the upper part of the slope, in which breaking and post-breaking are modeled and studied. Specifically, the internal values of the time derivative of the potential are computed with the BIE (2),(3), and the velocity field with the BIE (7),(8), based on the boundary solution. The pressure field is then obtained from Bernoulli equation.The interior control points of the BEM correspond to the centers of the VOF cells, so that it is easy to transfer velocity and pressure to the Navier-Stokes mesh. The VOF field is finally computed by interpolation, based on the shape of the BEM free surface.

Various types of incident waves can be specified in the BEM model. For solitary waves, for instrance, Tanaka's algorithm (Tanaka, 1986) provides a numerically exact shape and kinematics of the initial free surface, which is used to initialize the BEM model.

# NUMERICAL RESULTS

In this section, two examples of wave breaking simulations are presented. These are quasi-2-D cases, i.e., cases in which there is no variation along the transverse ($y$) direction in the 3-D model for both the incident wave and the bottom topography. Doing so, we will be able to directly compared 3-D and 2-D results. Other applications, with full 3-D variations are given in a companion paper (Biausser et al., 2003).

**Breaking of a linear wave**

The first application deals with the breaking of an initially large amplitude sinusoidal wave, in a periodic domain. This first test, although non-physically meaningful, is performed to check the capabilities of the 3D-SL-VOF method for simulating large deformations and reconnections of interfaces. For this test, the initial conditions on the free surface and the internal wave kinematics and pressure are obtained from linear wave theory. Hence, no coupling with the BEM model is required. The initial wave has a wavelength $L$ = 0.769 m, a period $T$ = 0.86 s, and height $H$ = 0.1 m. The computational domain is a 3-D box, one wavelength long, of depth $d$ = 0.1 m. Periodic boundary conditions are specified at the extremities of the domain. The wave is propagating in the x-direction. Due to the large initial ratio $H/d$, the wave is unstable and a strong plunging breaker rapidly develops in the VOF computations (Fig. 4). A breaker jet appears and impinges strongly on the forward free surface. After this splash-up, an ejection of fluid is observed (rebound), which falls back on the breaker jet.

As this breaking is quasi 2-D, it is interesting to analyze results in a vertical slice of the domain along the $x$-axis (Fig. 5). The modulus of the velocity is represented, and one can see that the largest velocities

are located in the breaker jet, as usually observed in breakers. This test-case confirms that the 3D-SL-VOF is able to track complex interfaces with accuracy and thus is a good tool to model with wave breaking.

**Breaking of a solitary wave**

The previous test-case qualitatively reproduced the process of breaking from simple initial conditions. However, the specified shape and ratio $H/d$ over a flat bottom for the initial wave did not correspond to a realistic wave train and, hence, the resulting wave breaking was somewhat artificial. In a second test-case, we model a more realistic breaking wave created by a sloping bottom, as occurs on most beaches. Here, the transfer from potential to kinetic energy during shoaling causes breaking, rather than non-physical initial conditions. Moreover, we produce breaking waves, whose characteristics now depend on both the wave profile and on the bottom slope geometry.

We thus model a 3-D domain, with a constant depth region followed by a sloping bottom (Fig. 6). Two sub-domains are considered, the first one corresponding to the flat bottom, from $x = 0$ to $x = 14$ m (with depth $h_0 = 1$ m), and the second one corresponds to a sloping bottom with a 1 : 15 slope from $x = 14$ m to $x = 35$ m, where shoaling of the wave is achieved, causing breaking of the wave. Let $H_0$ be the initial height of the wave, and $H_0' = H_0/h_0$. The initial wave is a numerically exact solitary wave (Tanaka, 1986), with $H_0' = 0.5$, and its crest is initially located at $x = 8.5$ m. The computational domain and the initial conditions are shown on Fig. 6.

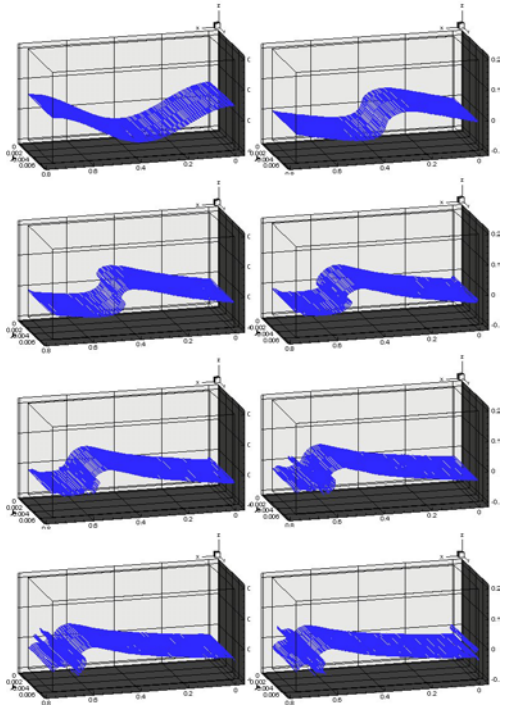

Figure 4: Large amplitude sinusoidal wave in a periodic domain. Evolution of the wave free surface in time.

In this application, no propagation is computed in the BEM model, which is only used to generate the initial conditions over constant depth, for the VOF/Navier Stokes (or Euler) solver, i.e., velocity and pressure fields, for the specified solitary wave shape and free surface kinematics. [Note, in other applications, presented in a companion paper (Biausser, et al., 2003), the wave is propagated in the BEM model up to close to breaking, hence, limiting the VOF computations to a much smaller and finely discretized box.]

As explained above, the VOF/Navier-Stokes solver is used here to compute the full shoaling and breaking of the wave. Viscous effects are neglected; hence Euler equations are solved rather than Navier-Stokes'. As previously discussed, breaking occurs as a result of shoaling over a non-uniform bottom topography. In this case, shown on Fig. 7, the wave progressively overturns, reaching the breaking point (where the crest front face becomes vertical) at $x = 27$ m. Eventually, a large size breaker jet is projected forward, producing a plunging type breaker. The breaking wave height is 0.45m.

As there are no variations of the slope in the transverse direction, the physical phenomenon is quasi 2-D. It is thus interesting to compare 3-D results obtained here, in a vertical cross-section along the direction of propagation, with 2-D VOF results, e.g., such as computed by Guignard et al. (1999,2001). The 2-D computational domain corresponds to a slice along the propagation direction of the 3-D domain. The same initial solitary wave is considered and the 2D-SL-VOF method is used (see Guignard et al., 1999, 2001 for details).

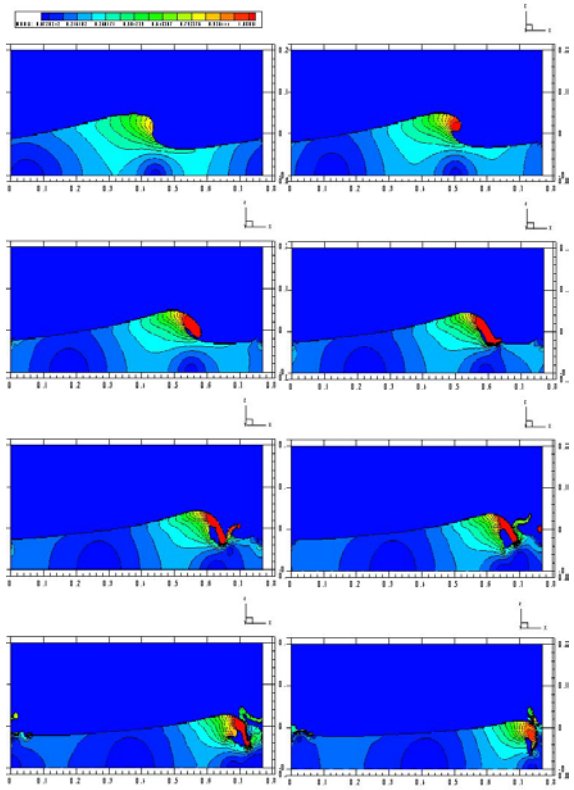

Figure 5 : modulus of the velocity in a vertical cross-section along the $x$-axis in Fig. 4

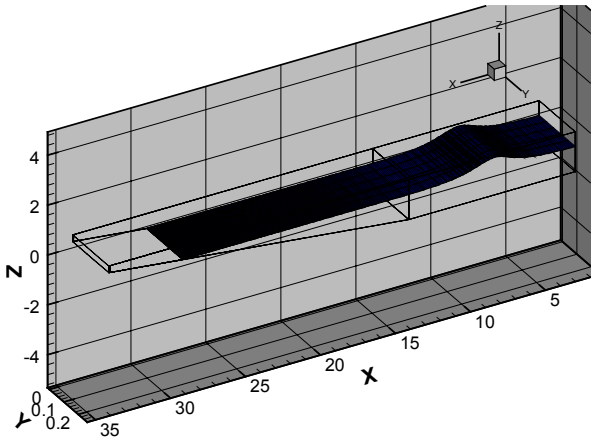


**Soliton 3D t=0 s : H/D=0.5, s=1/15**

Figure 6 : Initial conditions and computational domain for solitary wave shoaling and breaking over a 1:15 slope ($H_0'$ = 0.5).

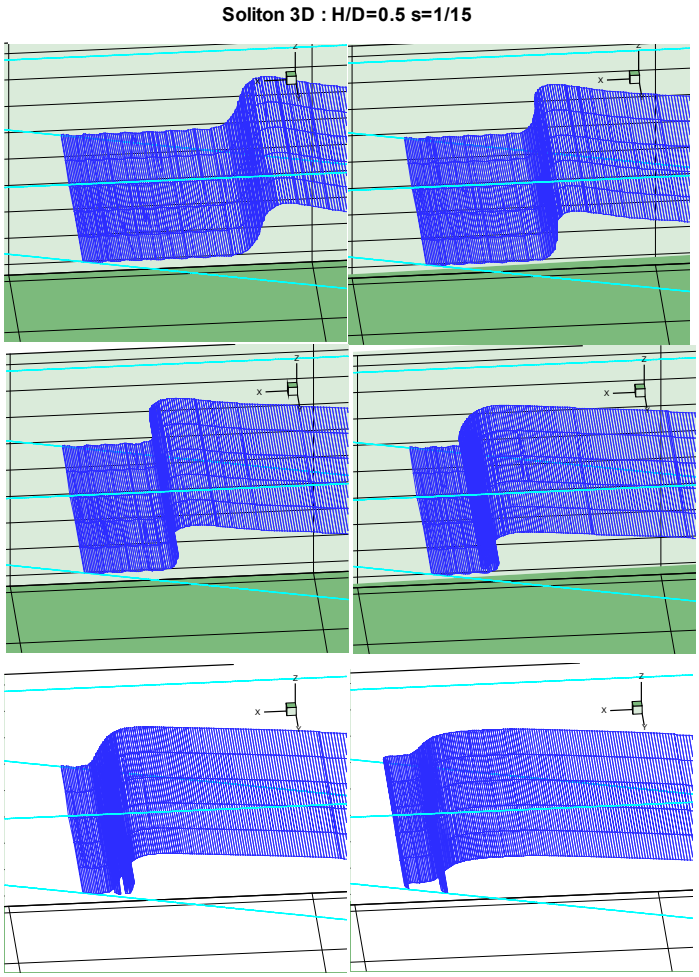


Figure 7 : breaking of the solitary wave over a sloping beach (case of Fig. 6, with $H_0'$ = 0.5).

The 2-D simulation results are shown on Figs 8a and b. As expected, the same phenomenon occurs, i.e., the creation of large size plunging breaker. Comparisons between the 2-D and 3-D simulations during breaking are presented on Fig. 9. One can see the strong similarity between the 2-D and 3-D simulation results. Small differences are only observed around the wave crest. Also, breaking occurs somewhat faster for the 2-D case. This is likely due to effects of discretization, which is coarser in the 3-D case and thus causes more numerical errors. Nevertheless, the overall shape of the breaker jets is very similar.

## CONCLUSIONS

The coupling between the SL-VOF and BEM methods for 2-D flows allowed Guignard et al. (1999,2001) to efficiently and accurately compute wave breaking on sloping beaches. In the present work, the extension of this coupling methodology to 3-D is presented and validated on two simple applications. Specifically, it is shown that the recently developed 3-D-SL-VOF method is also able to deal with large deformations of the interface and topological reconnections that occur during breaking, and hence is able to simulate 3-D wave breaking. The coupling with the 3-D-BEM method has been successfully achieved and gives results similar to results of the 2-D coupling for the case of a solitary wave shoaling and breaking on a sloping beach. Only initial VOF conditions, however, are calculated with the BEM. In a companion paper (Biausser et al., 2003), we both propagate waves up to close to breaking in the 3D-BEM model and we tackle truly 3-D breaking cases, over a slope, for which there is a transverse ($y$) modulation of the bottom topography, such as used in. Grilli et al. (2001).

Since the BEM method is more computationally efficient than the VOF method, a proper initialization at a later stage of wave propagation will significantly reduce computational time. Also, the VOF grid will be specified over a much smaller domain, hence allowing for a finer mesh size, thus reducing numerical errors and the (non-physical) loss of energy of waves during shoaling usually observed in VOF methods.

(a)

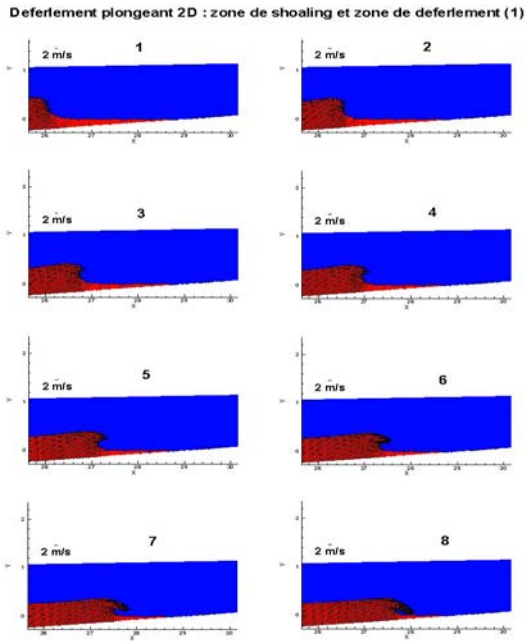

(b)

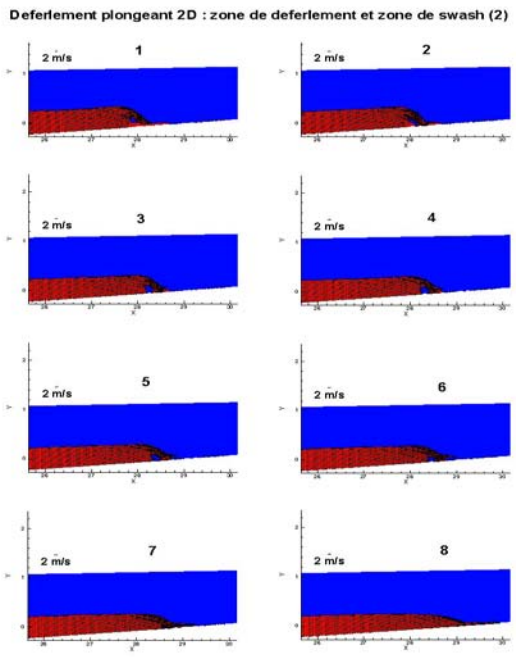


Figure 8 : Shoaling, breaking and post-breaking for 2-D simulations similar to Fig. 6 and 7

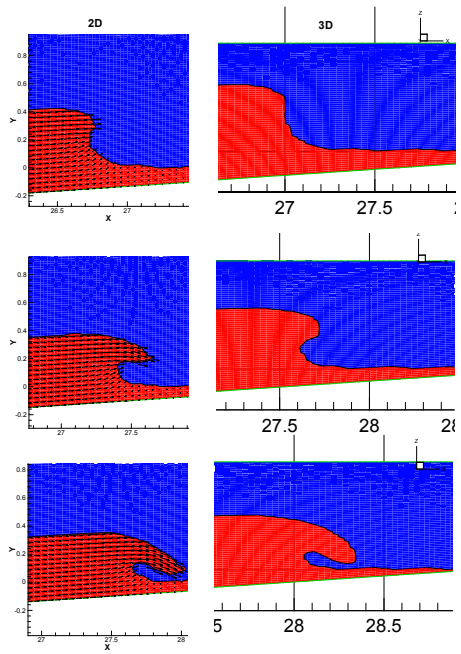


Figure 9: comparisons between 2-D and 3-D simulations in Figs. 7-8.

## REFERENCES


Biausser, B., Guignard, S., Marcer, R., Fraunié, P. (2001). "Numerical simulations of free surface flows using a new VOF method," *Proc. 4th Seminar Euler and Navier-Stokes Equations, Institute of Thermomechanics, Prague*.

Biausser, B., Guignard, S., Marcer, R., Fraunié, P. (2002). "3-D two-phase flows numerical simulations by SL-VOF method", *submitted for publication* .

Biausser, B., Grilli, S.T. and Fraunié, P. (2003). "Numerical Analysis of the Internal Kinematics and Dynamics of Three-dimensional Breaking Waves on Slopes", *Proc. 13th Offshore and Polar Engng. Conf.* (ISOPE03, Honolulu, HI, USA, May 2003), *submitted for publication.*.

Brandini, C. and S.T., Grilli (2001). "Modeling of freak wave generation in a 3D-NWT, " *In Proc. 11th Offshore and Polar Engng. Conf.* (ISOPE01, Stavanger, Norway, June 2001), Vol III, pp 124-131.

De Jouëtte, C., Viviand, H., Wornom, S. & Le Gouez, J.M. (1991). "Pseudo-Compressibility Methods for Incompressible Flow Calculation," *Proc 4th International Symposium on Computational Fluid Dynamics,University of California, Davis*.

Grilli, S.T., Guyenne, P. & Dias, F. (2001). "A fully nonlinear model forthree-dimensional overturning waves over arbitrary bottom," *Intl J. Numer. Meth. Fluids* , Vol 35, No 1, pp 829-867.

Grilli, S.T. and Horrillo, J. (1997). "Numerical Generation and Absorption of Fully Nonlinear Periodic Waves," *J. of Engng. Mechanics*, Vol. 123, No. 10, pp 1060-1069.

Grilli, S.T. and Horrillo, J. (1999). "Shoaling of periodic waves over barred-beaches in a fully nonlinear numerical wave tank," *Intl. J. Offshore and Polar Engng.*, Vol. 9, No. 4, pp 257-263

Grilli, S.T., & Subramanya, R (1996). "Numerical modeling of wave breaking induced by fixed or moving boundaries," *Computational Mech.*, Vol 17, pp 374-391.

Grilli, S., Subramanya, R., Svendsen, I.A. and Veeramony, J. (1994). "Shoaling of Solitary Waves on Plane Beaches." *J. Waterway Port Coastal and Ocean Engng.*, Vol 120, No 6, pp 609-628.

Grilli, S.T., Svendsen, I.A. and Subramanya, R. (1997). "Breaking Criterion and Characteristics for Solitary Waves on Slopes." *J. Waterway Port Coastal and Ocean Engng.*, Vol 123, No 3, pp 102-112.

Guignard, S., Grilli, S.T., Marcer, R. and Rey, V. (1999). "Computation of shoaling and breaking waves in nearshore areas by the coupling of BEM and VOF methods." In *Proc. 9th Offshore and Polar Engng. Conf.* (ISOPE99, Brest, France, May 1999), Vol. III, pp 304-309

Guignard, S., Marcer, R., Rey, V., Kharif, Ch. & Fraunié, P. (2001). "Solitary wave breaking on sloping beaches:2D two-phase flow numerical simulation by SL-VOF method". *Eur. J. Mech.*

Guyenne, P., Grilli, S.T. (2002). "Numerical study of three-dimensional overturning waves in shallow water", *submitted for publication.*.

Hirt, C.W., & Nichols, B.D. (1981). "Volume Of Fluid Method for the dynamics of free boundaries," *J.Comp. Phys.,* Vol 39, pp 323-345.

Jameson, A., Schmidt, W. & Turkel, E. (1981). "Numerical solutions of Euler equations by finite volume methods using Runge-Kutta time stepping schemes," *AIAA Paper 81-1259*.

Tanaka, M. (1986). "The stability of solitary waves," *Phys. Fluids,* Vol 29, No 3, pp 650-655.

Viviand, H. (1980). "Pseudo-unsteady Methods for Transonic Flow Computations," *19th International Conference on Numerical Methods in Fluid Dynamics, Stanford, in Lecture Notes in Physics,* Vol. 141, Springer-Verlag, New-York.

Viviand, H. (1995). "Analysis of pseudo-compressibility systems for compressible and incompressible flows," *Comp. Fluid Dynamics Review,Hafez-Oshima editor, Wiley publishers,* pp.399-418.

Xü, H, & Yue, D.K.P. (1992). "Computations of fully nonlinear three-dimensional water waves," *Proc. 19th Symp. On Naval Hydrodynamics, Seoul, Korea.*


## ACKNOWLEDGEMENT


The authors wish to acknowledge support from the French National Program PATOM (Programme Atmosphère et Océan à Multiéchelles).